



## Article

# Numerical Analysis on the Optimisation of Thermal Comfort Levels in an Office Located inside a Historical Building

Eleonora Palka Bayard de Volo <sup>\*</sup>, Beatrice Pulvirenti <sup>\*</sup>, Aminhossein Jahanbin , Paolo Guidorzi   
and Giovanni Semprini 

Department of Industrial Engineering, Alma Mater Studiorum University of Bologna, Viale Risorgimento 2, 40136 Bologna, Italy

\* Correspondence: eleonora.palkabayard2@unibo.it (E.P.B.d.V.); beatrice.pulvirenti@unibo.it (B.P.)

**Abstract:** The present study examines the possibility of thermal comfort optimisation inside an office room where, due to historical heritage, it is possible to modify neither the energetic characteristic of the envelope nor the position of the inlet air vents. The distribution of global and local thermal comfort indices is evaluated in both heating and cooling conditions by establishing a computational fluid dynamics (CFD) model validated against experimental data. The obtained results demonstrate a striking asymmetry of the air velocity and temperature distribution due to the low energy efficiency of the building. In heating mode, the predicted mean vote (*PMV*) values were improved if the discharged air from the fan coil was at its maximal velocity. However, at the same time, the vertical air temperature gradient increased by around 0.5 °C in each working station. In the cooling condition, in the absence of the solar radiation, the minimal air-flow rate satisfied the acceptable range of the draught rate (*DR*), whereas in the presence of a solar load, it could not meet the required cooling load in all positions, leading to higher floor temperature. The findings of this study allow for identifying and rearranging the optimal position of working stations in terms of thermal comfort.

**Keywords:** indoor environmental quality; thermal comfort; historical buildings; HVAC; numerical simulations; CFD



check for  
updates

**Citation:** Palka Bayard de Volo, E.; Pulvirenti, B.; Jahanbin, A.; Guidorzi, P.; Semprini, G. Numerical Analysis on the Optimisation of Thermal Comfort Levels in an Office Located inside a Historical Building. *Appl. Sci.* **2023**, *13*, 2954. <https://doi.org/10.3390/app13052954>

Academic Editor: Constantinos A. Balaras

Received: 7 February 2023

Revised: 21 February 2023

Accepted: 23 February 2023

Published: 25 February 2023



**Copyright:** © 2023 by the authors. Licensee MDPI, Basel, Switzerland. This article is an open access article distributed under the terms and conditions of the Creative Commons Attribution (CC BY) license (<https://creativecommons.org/licenses/by/4.0/>).

## 1. Introduction

Most industrialised countries are transitioning from a fossil-fuel-based economy to sustainable development. Thus, energy efficiency has become a common target for building designers and engineers. The preservation of a comfortable thermal environment in buildings is necessary to guarantee a pleasant experience for occupants. Indoor environmental quality (IEQ) plays an important role in occupants' daily life in terms of health, comfort, and well-being [1,2]. Since an individual spends most of the time in indoor environments, thermal comfort is a topic of interest in many types of facilities, such as educational, office, and residential buildings. Therefore, it is necessary to find solutions to maintain indoor thermal comfort and simultaneously minimise energy consumption in buildings. Many studies have proven that the physical environment of an office has significant effects on worker productivity [3], so that the more time that workers spend in the office, the more important it is to guarantee positive IEQ conditions.

For buildings with historical value, energy efficiency is a critical goal, since limitations on applicable energy solutions are imposed to preserve their aesthetic characteristics. Architectural constraints, often combined with economic difficulties, prevent the use of retrofitted technical solutions, causing high energy consumption and low indoor environmental quality. In this context, thermal comfort can be achieved with noninvasive strategies that include changing the input parameters of a heating and ventilation air conditioning (HVAC) system or strategically designing the interior furniture layout to better exploit thermal comfort areas. According to a survey of users of heritage buildings

on thermal perception, although thermal perception was poor, the users still preferred to adopt passive thermal comfort actions, such as wearing more clothes, rather than invasive retrofitting solutions that could be expensive and represent a potential loss in building value [4]. Chow et al. [5] designed a new air-conditioning (AC) technique to increase the air flow within a room, so that the summer temperature setting could be raised to use less energy, but still preserving a good level of thermal comfort. Zhuang et al. [6] built a CFD model to study the effects of furniture layout on indoor air quality in an office. Results showed that the furniture position significantly impacted indoor temperature and velocity distribution, so it is possible to improve breathing zones without changing HVAC terminals. Several researchers focused on the topic of buildings with historical heritage. M. Ealiwa et al. [7] compared the thermal comfort perceptions within an old and a modern building. That study indicated that people had an overall impression of higher thermal comfort in the old building than that in the newer building. J. Zagorskas et al. [8] covered the theme of retrofitting historical buildings when, due to a valuable façade or other heritage preservation requirements, only inside insulation is allowed.

The evaluation of thermal comfort is based on environmental and individual parameters. Thermal comfort can be evaluated with either the classical approach, which interprets the global and local thermal comfort via the predicted mean vote (*PMV*) and the predicted percentage dissatisfied (*PPD*) or adaptive approaches. The acquisition of the required data in order to evaluate thermal comfort is a time-demanding process that requires specific instruments to calculate the relevant environmental parameters. An interesting alternative technique to predict thermal comfort is CFD, which allows for evaluating the local distribution of the relevant parameters. In fact, CFD analysis is an important tool in the design phase to determine the internal layout, the operational mode of terminals (inlet temperature, air flow), and the position of sensors for room control systems [9,10]. Mashita et al. [11] combined CFD and machine learning to design an intelligent HVAC system capable of controlling the air temperature and velocity in different areas to create personalised thermal comfort areas for multiple users. Balocco [12] created a 3D model to analyse a palace in Italy for a future refurbishment project. In [13], the authors proposed plant refurbishment in a palace in Italy using CFD tools to simulate the energy performance of their solution. Corgnati et al. [14] used CFD to optimise the ventilation strategy and air distribution in a palace in Turin, Italy. A. Jahanbin et al. [15] analysed the efficacy of a HRV system coupled with a low-temperature radiator in satisfying IEQ indices inside a retrofitted dormitory room through CFD analysis, concluding that, while higher ventilation rates could significantly decrease the age of the air, this would cause local discomfort in some parts of the room. Later, in [16], the authors proposed a CFD model to investigate the effects of a combined MVHR–fan–coil system in heating mode on IAQ and thermal comfort parameters inside a retrofitted room.

The CFD method is abundantly applied to the evaluation of thermal comfort in different built environments. Nonetheless, there are few numerical studies in the literature addressing discomfort in historical buildings triggered by their particular thermophysical characteristics. In this context, this study proposes CFD analysis performed in multi-physics computational fluid dynamics software StarCCM+ (Siemens; Academic Power On Demand [17]) to evaluate the thermal comfort levels under summer-cooling and winter-heating conditions in an office inside a historical building of the Alma Mater Studiorum, University of Bologna, Italy. The building, designed by rationalist architect Giuseppe Vaccaro, was inaugurated in 1935. It is characterised by the presence of huge single-glazed glass windows that represent a critical component of the structure from a thermal point of view, due to their low thermal resistance and their low efficiency in filtering the sunlight. The methodology adopted for the study here presented is validated through a comparison with previous experimental measurement performed by [18]. In this previous study, Semprini et al. [18] performed thermal-comfort analysis of the same office room in winter-heating conditions, concluding that the internal layout of working desks should be rearranged. In particular, enough space between the working desks and the windows

should be given in order to satisfy local comfort. The obtained results in the present study allow for evaluating thermal comfort at different work stations in both winter and summer conditions, and for identifying discomfort zones that are related to the characteristics of the building and HVAC system. The focus of the analysis was to combine the global *PMV* index with local discomfort indices to obtain a more detailed evaluation of the level of comfort within the studied office.

## 2. Case Setup

The office is located on the first floor of the building and has the following geometrical dimensions:  $4.73 \times 5.03$  m, with a height of 4.24 m. As shown in Figure 1 the office is composed of two thick external masonry walls each containing a large window. The window in the southeastern direction occupies  $13.1 \text{ m}^2$ , while the one in the northwestern direction is smaller ( $7.5 \text{ m}^2$ ). Each window has a single-glazed glass with a thickness of 4 mm. The fan-coil unit is located under the SE window with an air exit surface of  $0.08 \times 0.65$  m ( $A = 0.052 \text{ m}^2$ ). Moreover, four different work stations are located inside the office room. For simplicity, 1 to 4 were assigned to each station to easily recall them in the following paragraphs.

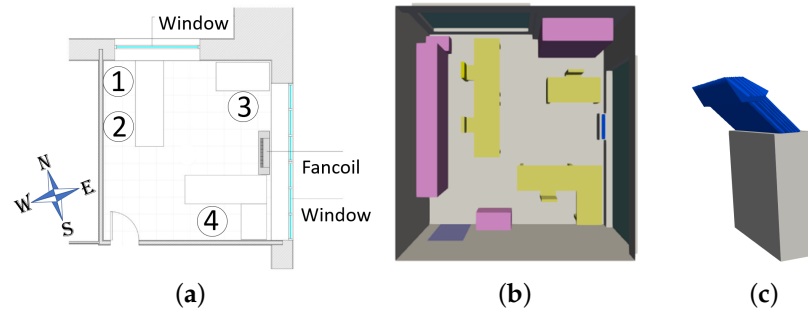


**Figure 1.** (a) Office schematic; (b) overview of the furniture layout inside the office; (c) fan-coil schematic with vector inlet at  $45^\circ$ .

The fan-coil unit works at three different air-flow rate levels corresponding to three different velocities of the inlet air. The minimum was 1 m/s and the maximum was 2 m/s. In this study, medium velocity of 1.5 m/s was not considered. The air was discharged with an angle of  $45^\circ$ , as shown in Figure 1c, at a temperature of  $16 \text{ }^\circ\text{C}$  during summer-cooling and at  $33 \text{ }^\circ\text{C}$  in winter-heating season. The HVAC system worked in a steady-state condition at the fixed inlet temperature of the fan coil since the local control system was not available.

The governing equations were the Mass (1), Momentum (2), and Energy (3) balance equations for steady-state, incompressible, and turbulent flows:

$$\vec{\nabla} \cdot \vec{v} = 0 \tag{1}$$

$$\rho_0 [(\vec{v} \cdot \vec{\nabla})\vec{v}] = -\nabla(p + \rho_0gz) + \rho_0g\beta(T - T_0)\nabla z + \vec{\nabla} \cdot \tau_{eff} \tag{2}$$

$$\vec{\nabla} \cdot [\vec{v}(\rho e + p)] = \vec{\nabla} \cdot [(k + k_t)\nabla T + \tau_{eff} \cdot \vec{v}] \tag{3}$$

where  $\vec{v}$  is the velocity vector,  $p$  is the pressure,  $\beta$  is the thermal expansion coefficient,  $\tau_{eff}$  is the effective stress tensor,  $e$  is the specific enthalpy,  $k$  is the thermal conductivity, and  $k_t$  the turbulent thermal conductivity.

The 3D governing differential equations were solved through the finite-volume method implemented through CFD software STARCCM+. A second-order upwind scheme was adopted to convert the governing equations into a set of algebraic discretized equations, and the semi-implicit method for pressure-linked equation (SIMPLE Algorithm) was

utilised to solve the pressure-velocity coupling problem. The convergence of the simulation solutions was monitored by controlling the values of residuals, velocity, and temperature on several randomly spread probes in the room. To optimise the solution convergence, linear under-relaxation factor ramps were used.

The Reynolds stress transport (RST) turbulence model and elliptic blending (near-wall Reynolds-stress turbulence closure) were used to best solve the involved turbulence. In this model, seven equations need to be solved: six equations for the Reynolds stresses (Equations (4) and (5); symmetric tensor) and one for the isotropic turbulent dissipation. Thus, the computational time is significantly increased with respect to the two equations models, but it can predict complex flows more accurately due to its capacity to naturally account for the effects of turbulence anisotropy (Lardeau et al. [19]).

$$T_{RANS} = -\rho R + \frac{2}{3} \text{tr}(R)I \quad (4)$$

where  $\rho$  is the density,  $I$  is the identity tensor, and  $R$  is the Reynolds stress tensor.

$$R = \begin{pmatrix} \overline{u'u'} & \overline{u'v'} & \overline{u'w'} \\ \overline{u'v'} & \overline{v'v'} & \overline{v'w'} \\ \overline{u'w'} & \overline{v'w'} & \overline{w'w'} \end{pmatrix} \quad (5)$$

Inlet air velocity at the exhaust vent of the fan-coil unit and a pressure outlet boundary condition is set on the outlet (located at the bottom of the fan-coil unit). The radiation heat transfer was considered by applying the surface-to-surface radiation model (Siegel, 1992) [20]. In this model, the air is considered a transparent medium, and all surfaces are assumed to be diffusive and grey. According to [18], the following values were considered for the emissivity of surfaces: 0.88, 0.89, 0.8, and 0.9 for the fan-coil box, window (glass), and walls, respectively. Boundary conditions of the third kind were applied at both the external walls and windows. The heat losses through the external walls and windows were estimated by considering thermal transmittance (U-values) equal to 1.4 and 5.7 W/(m<sup>2</sup>K), respectively, and a convection coefficient equal to 25 W/(m<sup>2</sup>K), while the remaining walls and the door were considered isothermal. Furthermore, the floor and ceiling surfaces were considered adiabatic.

The summer-cooling simulations were performed for a typical day of July when the outside temperature is 30 °C, while the isothermal internal walls are at a static temperature of 24 °C. Four different simulations were performed, varying the inlet air mass flow rate and the presence of the solar load. The values of the direct solar radiation (597.6 W/m<sup>2</sup> with a sunshine factor of 1) and diffuse solar radiation (597.6 W/m<sup>2</sup> with a diffuse fraction of 0.5) for 15 July 2021 were considered according to the solar-load tool of StarCCM+. When the solar load was disregarded, the direct radiation of the sun was set to 0, while low diffuse radiation of about 10 W/m<sup>2</sup> was considered due to the presence of a highly reflective adjacent building. The considered cases in this study are summarised in Table 1.

**Table 1.** Summary of the studied configurations in summer-cooling conditions.

	Season	Inlet Air Velocity (m/s)	Solar Load
Case A	Cooling	1	NO
Case B	Cooling	2	NO
Case C	Cooling	1	YES
Case D	Cooling	2	YES

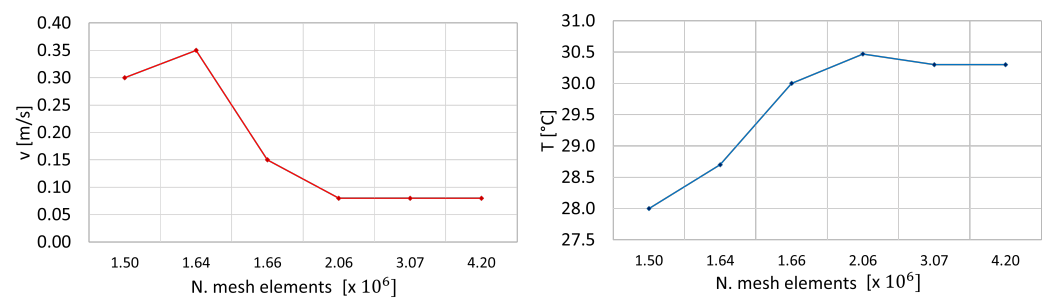
For the winter-heating simulations, 6 February 2021 was considered, when an external temperature of 6 °C was recorded. The isothermal internal walls were considered at a static temperature of 21 °C. The two studied cases only differed for the input air velocity and are summarised in Table 2.



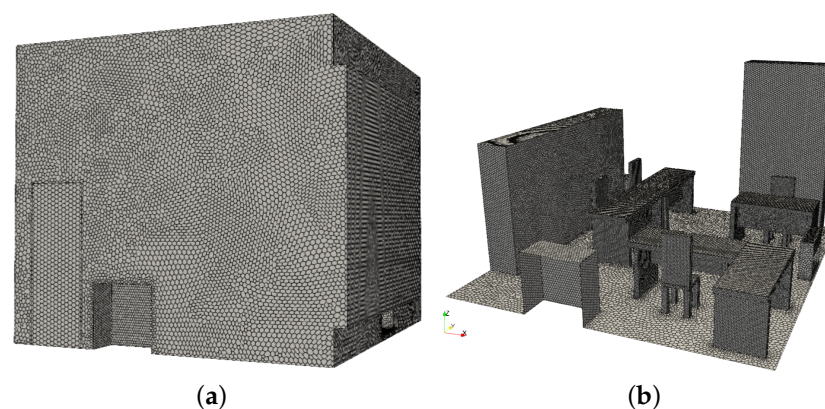
**Table 2.** Summary of the studied configurations in winter–eating conditions.

	Season	Inlet Air Velocity (m/s)	Solar Load
Case E	Heating	1	NO
Case F	Heating	2	NO

Mesh sensitivity analysis was performed to obtain the best scenario in terms of computational cost and accuracy of the results. Five different values of the base size of the mesh were considered. Velocity and temperature values in different positions inside the room were analysed. Figure 2 shows that the fourth mesh was the best choice in terms of trade-off between computational time and solution accuracy. Thus, the final mesh consisted of  $2 \times 10^6$  polyhedral elements with a base size of 6 cm.

**Figure 2.** Velocity and temperature values in one point obtained for the five different grids.

A nonuniform mesh strategy was regarded with a denser mesh in the vicinity of solid surfaces and fan-coil vents, and smoother mesh density with an expansion rate for far-field regions. A mesh refinement was performed on the furniture (4 cm) and chair (2 cm) surfaces due to their small geometrical dimensions with respect to the overall domain. In addition, a boundary layer was modelled in the fluid zone with five layers with a total thickness of 5% of the base size, resulting in a maximal  $y^+$  value of 3.5. An overview of the final mesh can be seen in Figure 3.

**Figure 3.** Final mesh. (a) View of the mesh from outside of the office; (b) view of the furniture.

The local parameters obtained with the simulations were used to evaluate the levels of discomfort inside the office with a focus on the working stations to define which the unfavourable ones were. In fact, the use of CFD allows for the prediction of these parameters even during the design of the HVAC system, so it is possible to evaluate the best operative conditions of the fan coil together with the distribution of the furniture inside the domain. The UNI EN ISO 7730:2005 [21] standard presents methods for predicting the general thermal sensation and the degree of discomfort (thermal dissatisfaction) of people exposed

to moderate thermal environments. Then, it is possible to evaluate the levels of comfort in enclosed environments by calculating the local discomfort parameters,  $e$  and predicted mean vote ( $PMV$ ) and associated predicted percentage dissatisfied ( $PPD$ ) values (Fanger, 1970) [22].

The single evaluation of the  $PMV$  usually tends to over- or underestimate the real thermal comfort perception, as reported by Rina Maiti (2014) [23], R. F. Rupp et al. [24], and K.W. Mui et al. [25]. As a global index, the  $PMV$  alone is not able to accurately recreate the real thermal perception since it does not account the possible effects of local discomfort felt by an occupant. Thus, we propose analysing local and global thermal comfort indices, and the effects of their combination for the evaluation of thermal comfort. According to the standard [21], Equations (6) and (7) allow for the evaluation of the dissatisfied percentage due to vertical air temperature gradients ( $PD_v$ ) and floor temperature ( $PD_f$ ), respectively.

$$PD_v = \frac{100}{1 + e^{(5.76 - 0.856\Delta T)}} \tag{6}$$

where  $\Delta T$  is the temperature difference in the range of a sitting person between their head (1.1 m) and ankles (0.1 m).

$$PD_f = 100 - 94e^{(-1.387 + 0.118T_f - 0.0025T_f^2)} \tag{7}$$

where  $T_f$  is the floor temperature.

Equation (8) allows for the identification of the drought rate ( $DR$ ) due to air flow.

$$DR = (34 - T_a)(v_a - 0.05)^{0.62}(0.37v_aT_u + 3.14) \tag{8}$$

where  $T_a$  is the air temperature,  $v_a$  is the air velocity, and  $T_u$  is the turbulence intensity. Equation (8) is only applicable when the air velocity is less than 0.5 m/s. CFD analysis allows for knowing the velocity values in each point of the domain. In this work, the velocity values were above the limit only in the zone right next to the fan-coil unit, so it was reasonable to use the  $DR$  equation in the rest of the room where the occupants were.

The  $PMV$  considers the body as a whole; thus, it differs from the previous indices and is a global parameter that depends on several parameters (Equation (9)). Some are environmental parameters, such as air temperature  $T_a$ , air velocity  $v_a$ , the water vapour partial pressure  $p_a$ , and mean radiant temperature  $T_{MR}$ . Others are individual parameters, which are metabolic rate  $Met$  and clothing insulation  $I_{clo}$ .

$$PMV = PMV(T_a, v_a, p_a, T_{MR}, Met, I_{clo}) \tag{9}$$

According to the standard [21] and related works, a  $Met$  rate of 1.2 and a  $I_{clo}$  of 0.5 [26] were assumed for people in a sitting position performing a sedentary activity during the summer season. For winter, a  $I_{clo}$  of 1 was considered instead [27].

The  $PMV$  classifies the environment in a scale from  $-3$  to  $+3$ , where  $0$  is a neutral condition in which occupants have the best thermal comfort perception, while  $-3$  and  $+3$  represent extreme sensations of cold and hot, respectively. Typically, the goal is to control environmental factors in order to keep the  $PMV$  value between  $-0.5$  and  $+0.5$ , where the body is thermally satisfied. The predicted percentage of dissatisfied ( $PPD$ ) related to the  $PMV$  values was evaluated according to the following empirical relationship in (10):

$$PPD = 100 - 95e^{-0.3353PMV^4 - 0.2179PMV^2} \tag{10}$$

Equations (9) and (10) were solved in a Python environment by using the pythermal-comfort utility created by [28]. Moreover, operative temperature values were calculated in

the room volume according to Equation (11), where  $T_a$  is the air temperature and  $T_{MR}$  is the mean radiant temperature within the room.

$$T_{op} = \frac{T_a + T_{MR}}{2} \tag{11}$$

### 3. Model Validation with Experimental Data

In order to validate the model, the simulation results were compared with our experimental measurements published in [18]. An innovative patented system was used to measure the position of the sensors within the office, as described in [29].

In order to evaluate the accuracy of the numerical model, 33 positions randomly spread inside the room (see Figure 4a) were considered, and temperature and velocity values were both compared with the profiles obtained via the simulation. Figure 4b shows the temperature values obtained with the measurements (considering an error bar of  $\pm 0.5\text{ }^\circ\text{C}$ ) compared with the corresponding values obtained with the simulation.

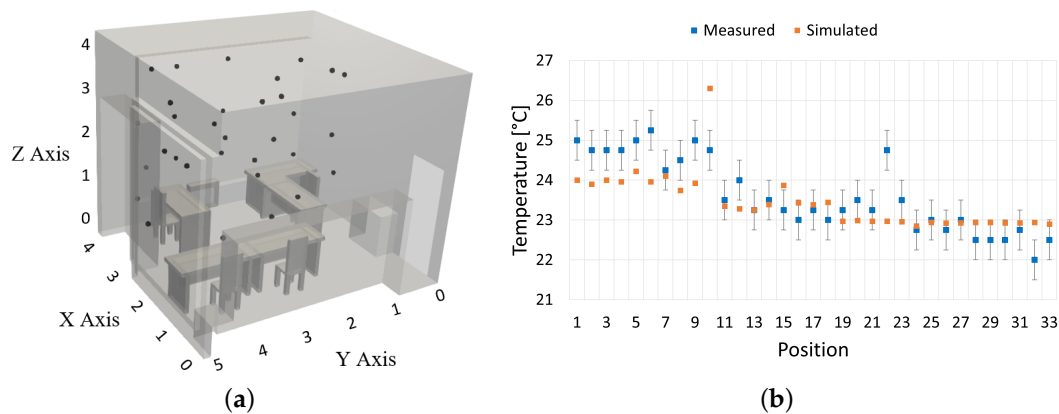


**Figure 4.** (a) Positions of the sensors for model validation. (b) Comparison of measured and simulated temperature values in the winter condition.

There was good agreement regarding temperature distribution with a mean relative error of about 2.2%. The highest relative errors of 6.3% and 7.2% were in Positions 22 and 10, respectively. Both these positions were located in the middle of the room at a height above 2.36 m. For the remaining positions, the measured and simulated values could be fully compared.

Table 3 shows the comparison between the measured and simulated air velocity values at different height and distances from the fan-coil unit.

**Table 3.** Comparison of measured and simulated velocity values.

Position	Distance from Fan Coil (m)	Distance from the Floor (m)	$v_{measured}(\frac{m}{s})$	$v_{simulated}(\frac{m}{s})$
a	0.6	1	0.05	0.05
b	0.6	1.5	0.11	0.10
c	0.6	2	0.52	0.48
d	1.1	1.5	0.01	0.02
e	1.1	2	0.02	0.03

The velocity values recorded from the set of measurements were reasonably modelled in the simulation. The above comparisons lead to the conclusion that the numerical model was validated, so any further change in the input parameters would return a trustable picture of reality.

## 4. Evaluation of Indoor Air Velocity and Temperature Distributions

### 4.1. Summer-Cooling Condition

The distribution of the air temperature and velocity obtained with numerical simulations is illustrated in Figures 5 and 6, respectively. When the minimal inlet air velocity was set to 1 m/s and no solar load was considered, the discharged air from the fan-coil unit tended to move towards the floor due to lower density after flowing around a meter (Figure 5, Case A). By increasing the inlet velocity, the forced convection condition was prevalent, and the discharged air from the fan coil moved directly until it had hit the opposite wall, which is demonstrated in Figure 5, Case B. When solar radiation was present, the temperature difference between inlet air and surrounding environment was rather large; thus, the air around the fan coil was mostly driven by buoyancy force upwards. In this case, the inlet air of the fan coil tended to move towards the floor sooner than other cases did, and less fresh air was delivered to Positions 1 and 2 (see Figure 1, Case A) than that in the other cases (Figure 5, Case C). The streamlines of Case D showed a rather similar trend to that in Case B with an augmented natural convection effect due to solar radiation.

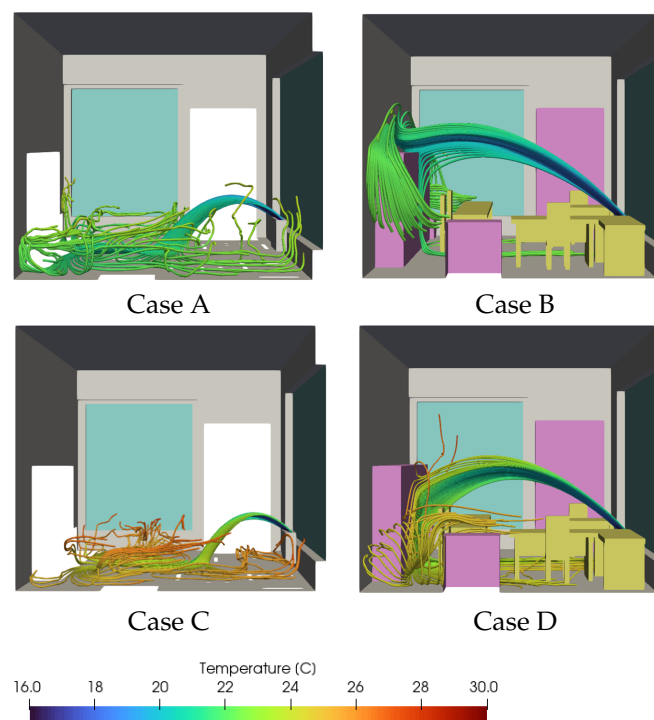


**Figure 5.** View from the entrance of the streamlines obtained for summer cooling with low input air velocity and no solar load (Case A), high input air velocity and no solar load (Case B), low input air velocity and solar load (Case C), high input air velocity and solar load (Case D).

The resulting temperature profile inside the office was characterised by important nonuniformity along the different working stations, as shown in Figure 6. When the solar load was taken into account, the case with minimal inlet air flow could not satisfy the required thermal field to cool the environment, and this resulted in the worst possible situation. The following mean static air temperature and mean operative temperature values were obtained for each case:  $T_{mean} = 24.1$  °C,  $T_{op} = 24.6$  °C for Case A,  $T_{mean} = 22.8$  °C,  $T_{op} = 23.6$  °C for Case B,  $T_{mean} = 27.6$  °C,  $T_{op} = 28.1$  °C for Case C and  $T_{mean} = 26.1$  °C,  $T_{op} = 27.0$  °C for Case D. Thus, an incident radiation impact of about 4 °C in mean temperature was obtained in the room.

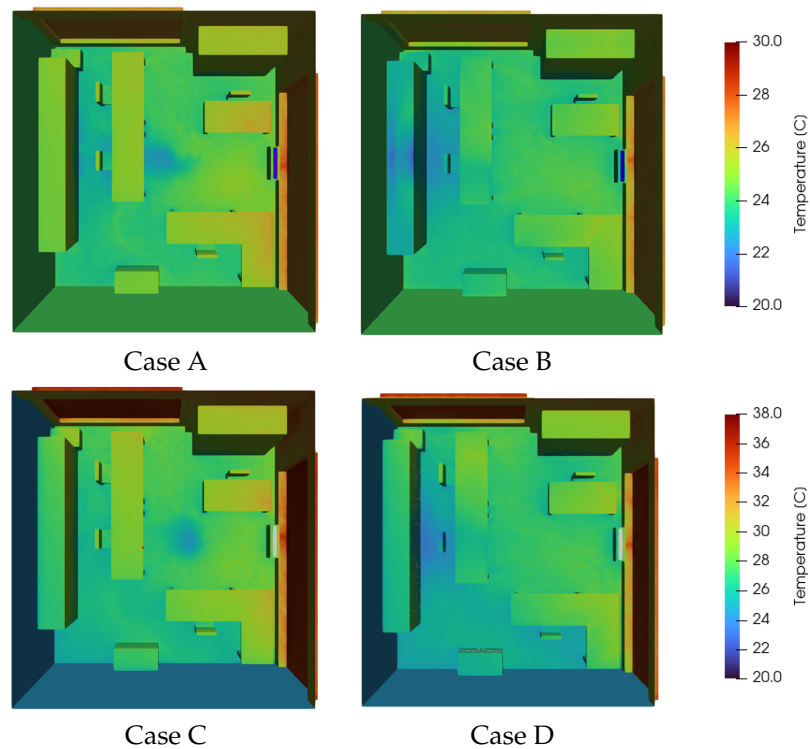


**Figure 6.** Top view of the internal temperature profile obtained in summer with low input air velocity and no solar load (Case A), high input air velocity and no solar load (Case B), low input air velocity and solar load (Case C), high input air velocity and solar load (Case D).

#### 4.2. Winter-Heating Condition

The winter-heating condition completely differed from the summer-cooling one, since the buoyancy effect on the input air forced the flow to follow the injection direction up to the ceiling, as shown in Figure 7. As a matter of fact, Cases E and F both avoided air flows that directly impacted the stations. This air distribution resulted in a massive stratification of the temperature within the office. The mean static air temperature and mean operative temperature values obtained for these cases were  $T_{mean} = 22.6\text{ }^{\circ}\text{C}$ ,  $T_{op} = 21.8\text{ }^{\circ}\text{C}$  for Case E and  $T_{mean} = 24.5\text{ }^{\circ}\text{C}$ ,  $T_{op} = 23.1\text{ }^{\circ}\text{C}$  for Case F but Figure 8 shows that the temperature on the internal furniture and walls was much lower.

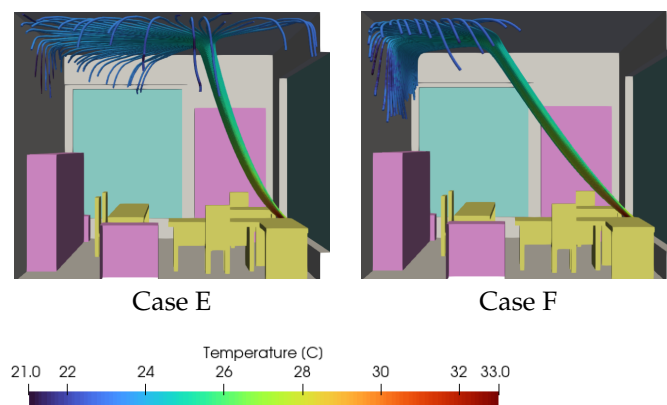


**Figure 7.** View from the entrance of the streamlines obtained for winter heating with low input air velocity (Case E) and high input air velocity (Case F).



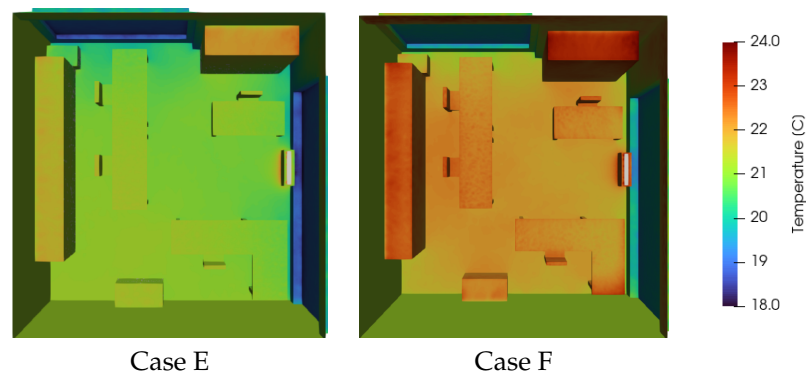
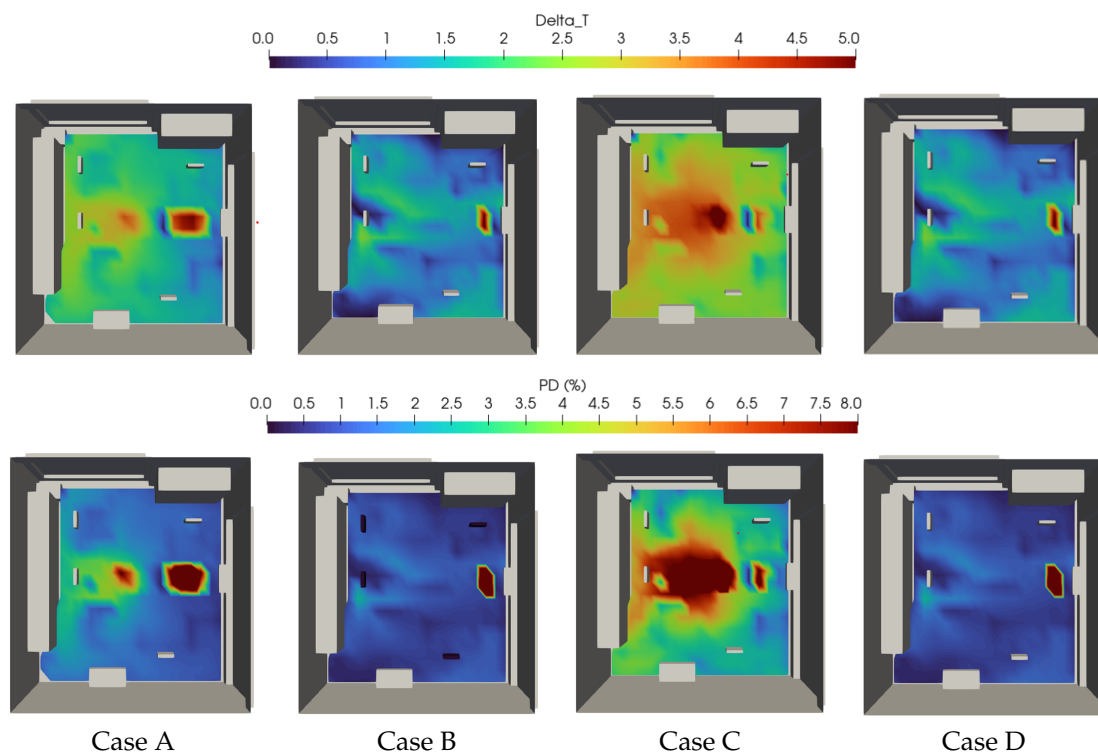


**Figure 8.** Top view of the internal temperature profile obtained for winter heating with low input air velocity (Case E) and high input air velocity (Case F).

### 5. Evaluation of Local Discomfort Indexes and PMV

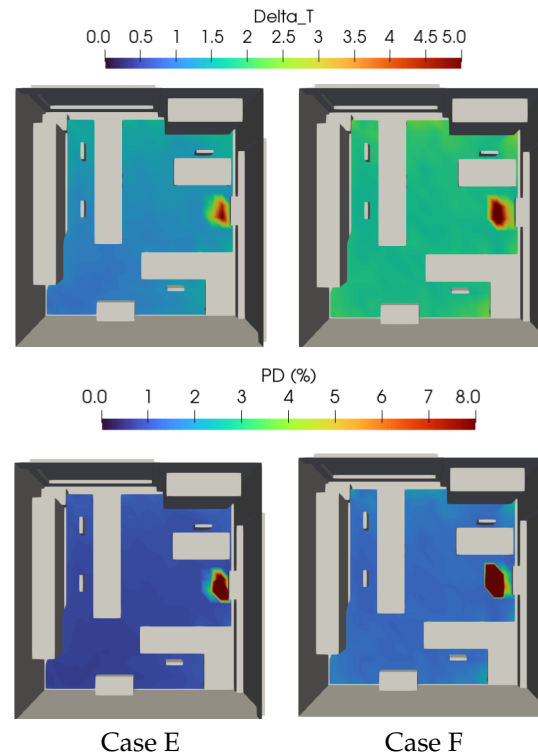
#### 5.1. Dissatisfied Percentage Related to Vertical Air Temperature Gradients

Figure 9 demonstrates the vertical air temperature gradients and relative percentage of dissatisfied for the summer configurations. It shows that when the temperature gradient is  $\Delta T < 3\text{ }^\circ\text{C}$ , the percentage of dissatisfied is  $PD_v < 4\%$  which is considered as comfortable condition for occupants. According to Figure 9, the highest air temperature gradients along the z axis was associated with the minimal inlet air-flow rate, especially when solar radiation was accounted for (Case C). At the minimal flow rate of the fan coil, Stations 2 and 3 were the zones with the most discomfort in terms of  $PD_v$ . The results indicate that, when the inlet air-flow rate was set at the maximum, the distribution of  $PD_v$  was more uniform, and the comfort condition was dominant in both the case with and that without solar radiation.



**Figure 9.** Summer cooling condition. Vertical air temperature gradients (top subfigures) and relative percentage of dissatisfied (bottom subfigures) obtained for low input air velocity and no solar load (Case A), high input air velocity and no solar load (Case B), low input air velocity and solar load (Case C), high input air velocity and solar load (Case D).

During winter condition, the situation was inverted. There were lower values of  $PD_v$  where the minimal air flow rate was accounted for, as shown in Figure 10. In fact, Case F presents values of  $\Delta T$  that ranged from 2 to 3 °C all over the office except for the zone where the fan coil was located. Case E, instead, had a  $\Delta T$  of 1 and 2 °C with a consequent  $PD_v < 1\%$ .



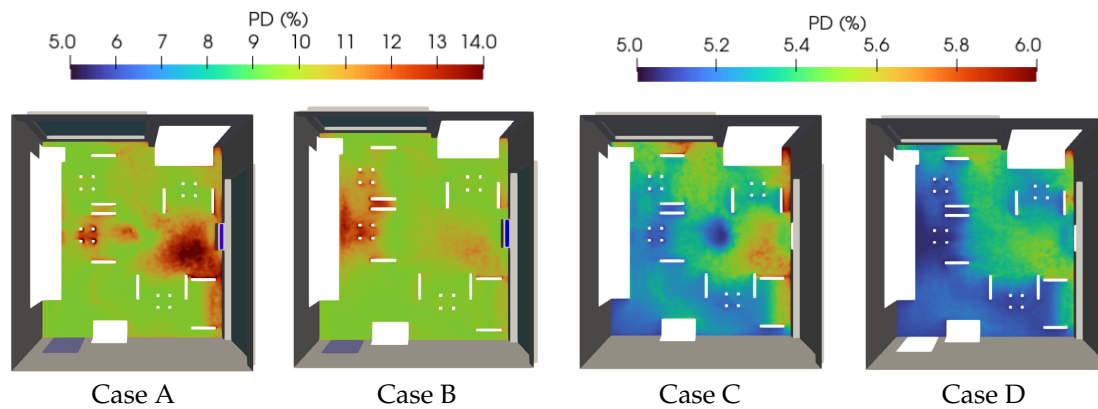
**Figure 10.** Winter heating condition. Vertical air temperature gradients (top subfigures) and relative percentage of dissatisfied (bottom subfigures) obtained with low input air velocity (Case E) and high input air velocity (Case F).

### 5.2. Percentage of Dissatisfied Related to Floor Temperature

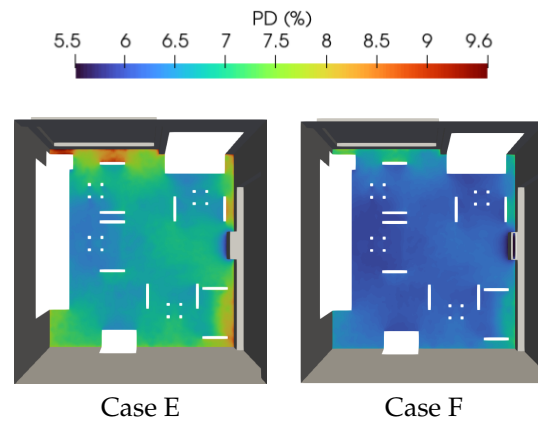
According to the standard [21], the ideal floor temperature is 24 °C with an associated minimal percentage of dissatisfaction  $PD_f = 5\%$ . Cooler or hotter floor temperatures lead to higher values of  $PD_f$ .

Figure 11 shows the percentage of dissatisfied distribution along the office floor obtained for the summer-cooling cases. When no solar load was considered, both inlet air velocities could guarantee a pleasant floor temperature; in the presence of the solar radiation, the floor temperature increased to some extent and lead to a higher percentage of dissatisfied. The worst result in this context was obtained for Case C, namely, minimal inlet velocity with a solar radiation load.

In the same way, Figure 12 shows the distribution of  $PD_f$  associated with floor temperature in the winter-cooling condition. For both cases (minimal and maximal inlet air velocities), the highest values of  $PD_f$  were found near the external walls; Case E had the highest discomfort for floor temperature.



**Figure 11.** Summer cooling conditions. Percentage of dissatisfied distribution along the office floor obtained for low input air velocity and no solar load (Case A), high input air velocity and no solar load (Case B), low input air velocity and solar load (Case C), high input air velocity and solar load (Case D).

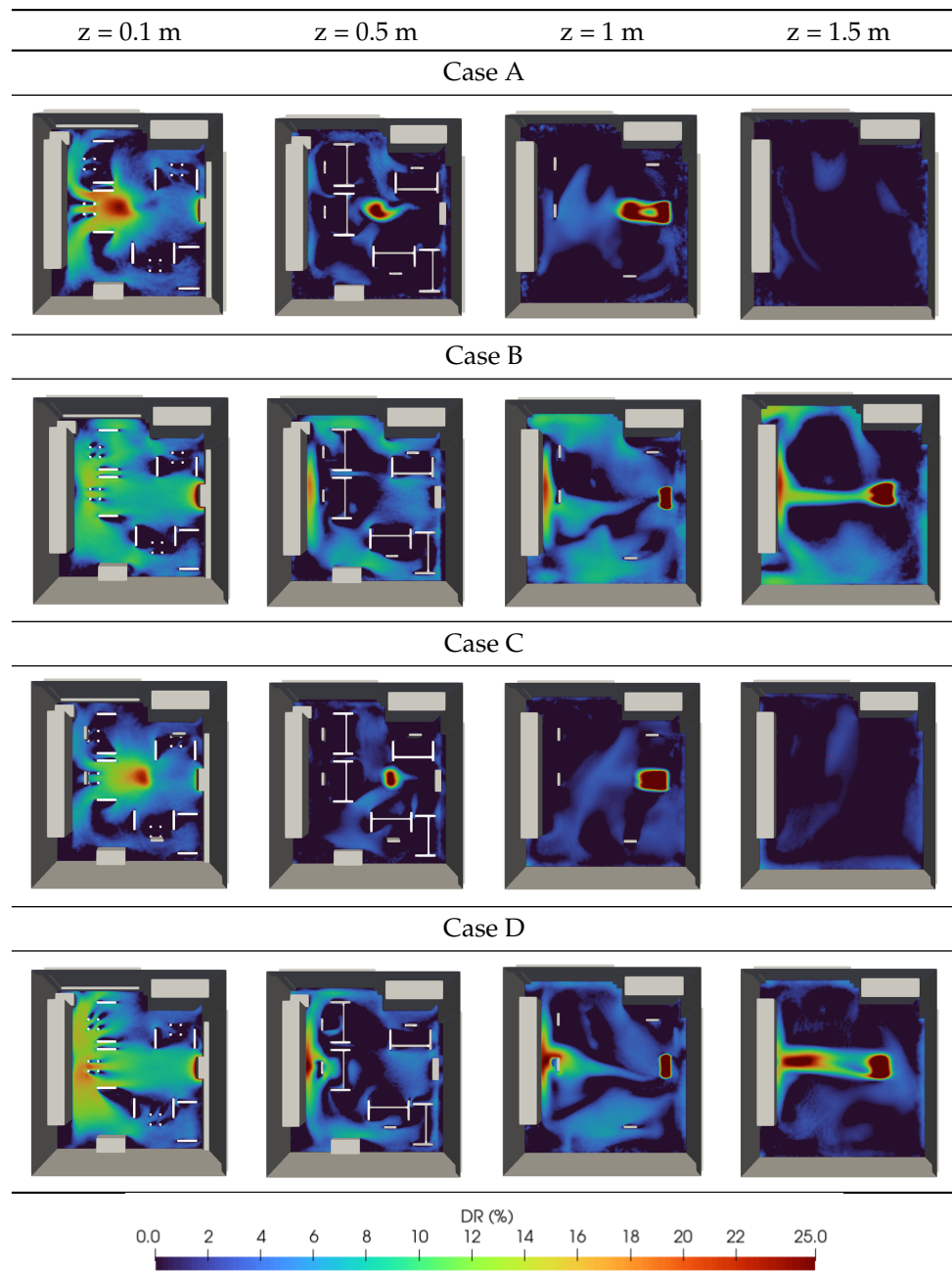


**Figure 12.** Winter heating condition. Percentage of dissatisfied distribution along the office floor obtained with low input air velocity (Case E) and high input air velocity (Case F).

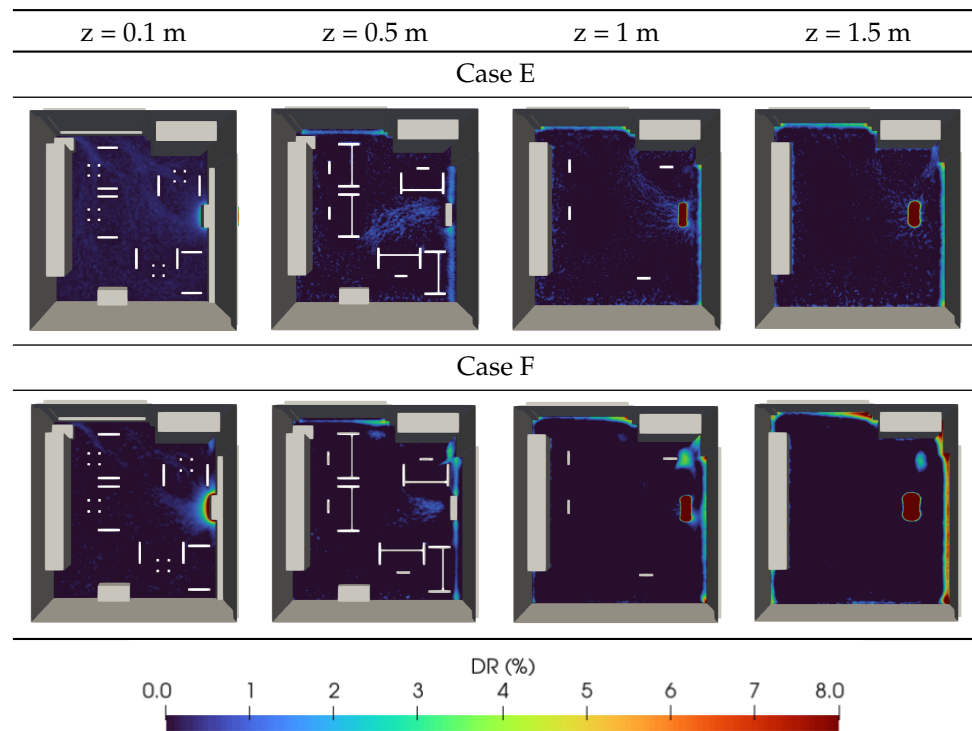
### 5.3. Draught Rate Related to Air Flows

Figure 13 compares the *DR* profiles of different sections in the *z* direction obtained for each summer case. It shows that Working Stations 1 and 2 were the most unfavourable in terms of *DR*, which was due to their placement at opposite sides of the fan coil. In fact, in these zones, *DR* values reached more than 20% in the zones of the ankles (0.1 m) and neck (1 m).

In the same way, Figure 14 shows the *DR* distribution at the same heights for the winter-heating condition. In these cases, the buoyancy effect on the discharged hot air lead to more uniform velocity distribution at human height with consequent low *DR* values.



**Figure 13.** Summer cooling condition. Draught-rate profile on different sections in the z direction obtained for low input air velocity and no solar load (Case A), high input air velocity and no solar load (Case B), low input air velocity and solar load (Case C), high input air velocity and solar load (Case D).



**Figure 14.** Winter heating condition. Draught-rate profile on different sections in the  $z$  direction obtained with low input air velocity (Case E) and high input air velocity (Case F).

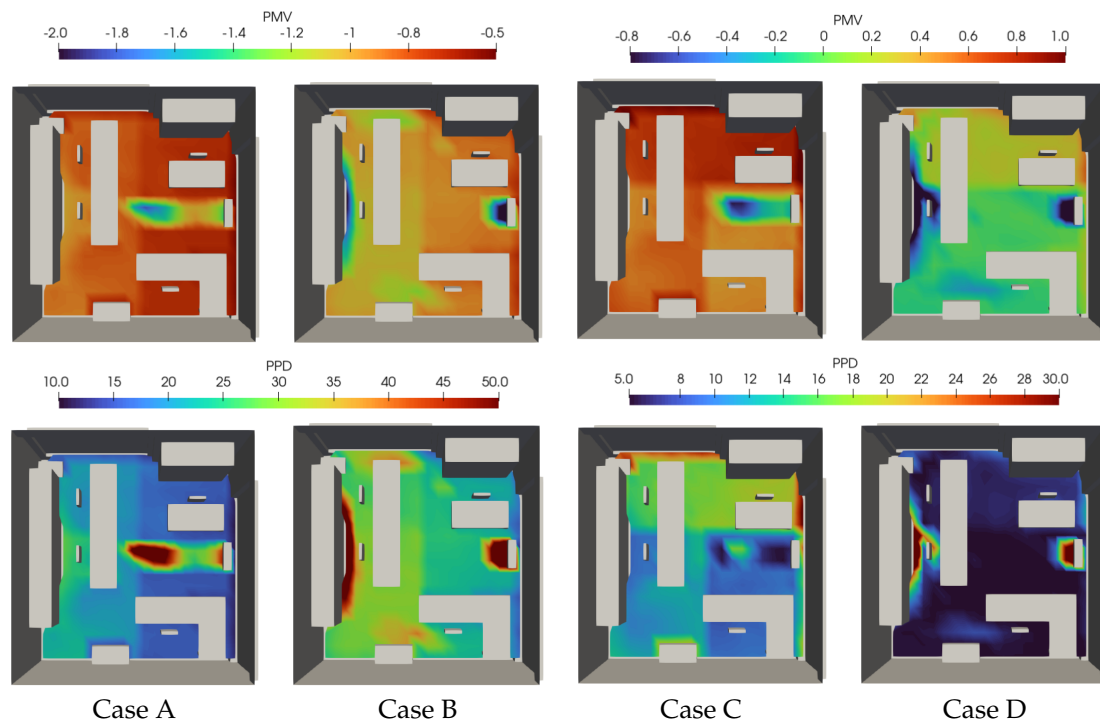
#### 5.4. Predicted Mean Vote and Predicted Percentage of Dissatisfied

Figure 15 illustrates  $PMV$  and  $PPD$  values inside the office for summer-cooling cases. The figure shows that, when the solar load was disregarded, the left zone of the office (where Stations 1 and 2 were located) was rather cool with larger  $PPD$  values compared to those in the right zone. This effect was amplified when the inlet air-flow rate increased, so Case B had the highest dissatisfied percentage. When solar radiation was applied, the situation changed: the minimal air-flow rate was not able to provide the necessary thermal power to balance the heat flux. Therefore, the entire environment was hot (except for the zone adjacent to the fan coil). In this case, the highest  $PPD$  (30%) was near the SE window, so Station 1 was the worst place in terms of thermal comfort. Case D on the other hand, presented a rather low  $PMV$  value in the zone of Station 2, varying from 0.6 to 1.4, representing a cold sensation. In the rest of the domain, a neutral-to-rather-hot sensation prevailed.

Figure 16 shows the  $PMV$  and associated  $PPD$  distribution in the office during winter-heating conditions. Both cases (minimal and maximal inlet air velocities) ensured a pleasant experience for the occupants, with  $PMV$  values that ranged from  $-0.5$  to  $0.1$ . In particular, Case F had the best environmental condition for thermal comfort, with  $PMV$  values close to 0 all over the office. For both cases, a slight cold sensation was felt near the windows, especially the one on the northeastern direction; so, it was reasonable to move the working stations, so that they were not too close to them.

Overall, in both summer and winter conditions, there was strong asymmetry in terms of  $PMV$  due to the low thermal efficiency of the building envelope.





**Figure 15.** Summer cooling condition. *PMV* (top subfigures) and relative *PPD* (bottom subfigures) distributions in the office obtained for low input air velocity and no solar load (Case A), high input air velocity and no solar load (Case B), low input air velocity and solar load (Case C), high input air velocity and solar load (Case D).

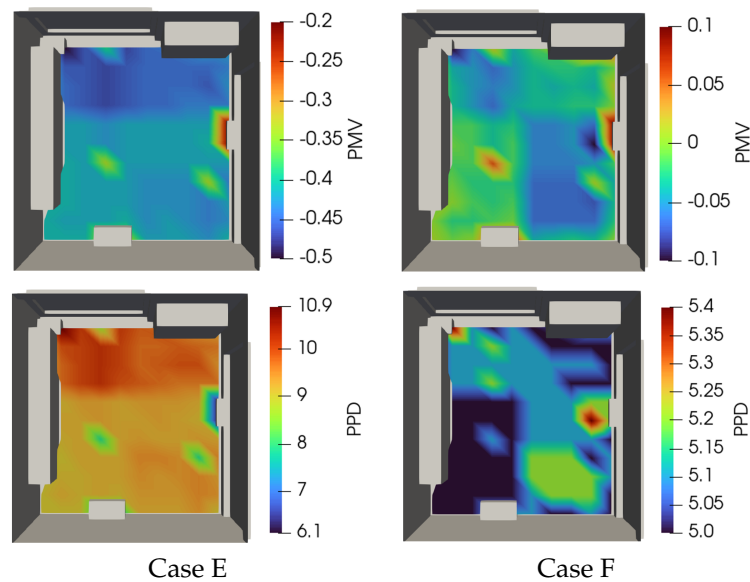


**Figure 16.** Winter heating condition. *PMV* (top subfigures) and relative *PPD* (bottom subfigures) distributions along the office obtained with low input air velocity (Case E) and high input air velocity (Case F).

### 6. Discussion

The different indicators considered above were evaluated and compared at different positions (see Figure 1a), as shown in Table 4. In particular, *PMV* and associated *PPD* values were tabulated together with the critical values of the local discomfort indices found in the four stations. The last column of the table contains the overall environment class obtained combining the different indicator categories according to [21].

**Table 4.** *PMV*, associated *PPD*, and critical values of local discomfort indices for each case at the four working stations. Categories of the thermal environment.

STATION 1								
	<i>PMV</i>	<i>PPD</i> (%)	<i>DR</i> (%)	$T_f$ (°C)	$PD_f$ (%)	$\Delta T$	$PD_v$ (%)	Category
Case A	−0.9	20.6	9.5	24.0	5.6	2.5	2.5	C
Case B	−1.1	29.7	14.3	23.5	5.9	1.7	1.3	C
Case C	0.7	15.7	5.9	28.4	10.8	3.3	4.8	C
Case D	0.1	6.5	16.1	26.6	7.6	1.7	1.3	B
Case E	−0.5	9.9	2.0	22.9	5.6	1.5	1.1	B
Case F	−0.1	5.1	0.9	23.4	5.5	2.1	1.8	A
STATION 2								
	<i>PMV</i>	<i>PPD</i> (%)	<i>DR</i> (%)	$T_f$ (°C)	$PD_f$ (%)	$\Delta T$	$PD_v$ (%)	Category
Case A	−1.0	25.4	15.5	23.6	6.3	3.0	3.8	C
Case B	−1.3	42.3	20.9	23.2	6.0	2.5	2.5	C
Case C	0.5	10.0	8.8	26.8	7.9	3.8	7.6	C
Case D	−0.7	20.3	25.7	25.3	6.2	2.5	2.5	C
Case E	−0.5	9.2	1.9	21.8	6.3	1.2	0.9	B
Case F	0.0	5.0	1.7	22.7	5.7	1.8	1.5	A
STATION 3								
	<i>PMV</i>	<i>PPD</i> (%)	<i>DR</i> (%)	$T_f$ (°C)	$PD_f$ (%)	$\Delta T$	$PD_v$ (%)	Category
Case A	−0.7	15.2	4.7	24.6	5.7	1.9	1.5	C
Case B	−0.9	21.6	10.1	24.1	5.6	1.1	0.8	C
Case C	0.8	19.2	2.4	28.6	11.3	2.7	3.0	C
Case D	0.3	6.9	4.5	27.7	9.5	1.1	0.8	B
Case E	−0.5	9.8	1.3	23.4	5.7	1.6	1.2	B
Case F	−0.1	5.1	5.8	23.9	5.5	2.1	1.9	A
STATION 4								
	<i>PMV</i>	<i>PPD</i> (%)	<i>DR</i> (%)	$T_f$ (°C)	$PD_f$ (%)	$\Delta T$	$PD_v$ (%)	Category
Case A	−0.7	15.4	2.8	24.1	5.6	1.8	1.4	C
Case B	−0.9	22.2	8.4	23.9	5.6	1.4	1.0	C
Case C	0.4	8.8	4.6	27.2	8.6	2.9	3.7	B
Case D	−0.1	5.2	6.4	26.6	7.6	1.4	1.0	A
Case E	−0.5	9.3	0.8	23.5	5.6	1.3	1.0	B
Case F	−0.1	5.2	0.1	23.8	5.5	1.8	1.5	A

During summer, when no solar load was accounted for, both the minimal and the maximal velocities of the discharged air resulted in a slight cold sensation. The higher the input air velocity was, the higher the *PPD* and *DR* values were. Overall, all the stations were Class C for Cases A and B. On the other hand, when a solar load was applied, the minimal inlet air velocity could not deliver enough fresh air to Stations 1 and 2, leading to a slight hot sensation. In addition, high values of floor temperature were found near Stations 1 and 3, leading to  $PD_f$  values higher than 10% (Class C). Station 2 had the highest value of vertical air temperature difference found in this study, about 7.6 °C, far above the maximal allowable value of 3 °C (Class C). The remaining stations had a high vertical air temperature gradient as well, which brought them into Class B. By increasing the input air velocity, the situation changed, and an overall cold sensation was felt except for Station 3. This station was placed right next to the window, so that it could capture more thermal radiation.

During winter, a much more uniform distribution of *PMV* and *PPD* values was found within the room. High *DR* values were avoided given the buoyancy effects on discharged air flows. Thus, the classification was mostly driven by the values of *PMV* and *PPD*, since no local discomfort was detected in the room. By increasing the discharged air velocity, *PMV* values were improved, while  $PD_v$  values associated with vertical temperature gradients rose by about 5 °C in each working station. All the working stations were Class A

when a high value of discharged air velocity was considered (Case F), and Class B when the minimal inlet air velocity was applied (Case E).

## 7. Conclusions

In the present study, a CFD code was established and validated against measured data to analyse the thermal-comfort levels in a historical office building. Four different summer scenarios were studied by considering two inlet flow rates of the fan coil, with and without solar irradiation, and two scenarios varying the inlet air-flow rate during winter. Different local discomfort indices, in addition to the predicted mean vote (*PMV*) and predicted percentage of dissatisfied (*PPD*), were evaluated for each case study to identify the occupants' thermal perception at different zones. The obtained results allowed for finding discomfort zones due to the studied building characteristics and cooling system, and working places in which better thermal comfort could be obtained. The findings of the present study provide insights into achieving better thermal comfort condition inside offices located in buildings with historical value. According to the results of the numerical simulations, the following conclusions were reached:

- Solar irradiation was the most influential parameter in terms of thermal comfort inside the office in summer-cooling conditions. It was important to weaken its effects by adopting a tent or by employing more efficient windows. As was observed for winter, working stations should be rearranged, so that enough space is left from the windows to avoid direct solar radiation to the desks.
- In summer, in the absence of solar radiation, the higher inlet air-flow rate of fan coil caused a significant increase in the percentage of discomfort due to the draught rate. Therefore, it is reasonable to use a low and at the same time reduce energy consumption.
- Among different summer case studies, the case with a higher inlet flow rate of fan coil in the presence of solar radiation had the lowest values of *PPD* inside the room. Moreover, Station 2 was directly intercepted by the discharged air flow, and a high value of *DR* was found.
- During winter, the distribution of the thermal comfort parameters was much more uniform. A high inlet air-flow rate improved the *PMV* values, but the values of  $PD_v$  associated with vertical temperature gradients increased with respect to the minimal discharged air velocity. Enough space should be left between the working stations and external walls to avoid possible local discomfort due to floor temperature.

The results show that the low energy efficiency of historical buildings results in the intensive asymmetry of indoor air velocity and temperature distribution, especially during summer, so different degrees of comfort were found in different working places within the room. The findings of this study allow for identifying and rearranging the optimal position of working stations in terms of the thermal comfort during both heating and cooling seasons. The adopted multiobjective optimisation is a low-cost solution for the improvement of thermal comfort in buildings with historical value where the energy demand is immense and there is no possibility to modify the energy characteristics of the envelope.

**Author Contributions:** Conceptualisation, B.P., G.S., A.J., P.G. and E.P.B.d.V.; methodology, E.P.B.d.V., A.J., and B.P.; software, E.P.B.d.V.; validation, E.P.B.d.V. and P.G.; formal analysis, E.P.B.d.V. and B.P.; investigation, E.P.B.d.V.; data curation, E.P.B.d.V.; writing—original draft preparation, E.P.B.d.V., A.J., and B.P.; writing—review and editing, E.P.B.d.V., A.J., and B.P.; supervision, A.J., B.P., G.S., and P.G. All authors have read and agreed to the published version of the manuscript.

**Funding:** This research received no external funding.

**Institutional Review Board Statement:** This study does not require ethical approval.

**Informed Consent Statement:** Not applicable.

**Data Availability Statement:** Not available.

**Conflicts of Interest:** The authors declare no conflict of interest.

### Abbreviations

The following abbreviations and symbols are used in this manuscript:

CFD	Computational fluid dynamics
HVAC	Heating, ventilation, and air conditioning
AC	Air conditioning
PMV	Predicted mean vote
PPD	Predicted percentage of dissatisfaction
$PD_v$	Percentage of dissatisfaction due to vertical air temperature gradients
$PD_f$	Percentage of dissatisfaction due to floor temperature
DR	Drought rate
Met	Metabolic rate
$I_{clo}$	Clothing insulation coefficient

### Greek and Latin symbols

A	Surface area (m <sup>2</sup> )
$v$	Velocity magnitude (m s <sup>-1</sup> )
$p$	Pressure (Pa)
$\rho$	Fluid density (kg m <sup>-3</sup> )
$\rho_0$	Reference fluid density (kg m <sup>-3</sup> )
$\beta$	Thermal expansion coefficient (K <sup>-1</sup> )
$\tau_{eff}$	Effective stress tensor (Pa)
$e$	Specific enthalpy (J kg <sup>-1</sup> )
$k$	Thermal conductivity (W m <sup>-1</sup> K <sup>-1</sup> )
$k_t$	Turbulent thermal conductivity (W m <sup>-1</sup> K <sup>-1</sup> )
$R$	Reynold stress tensor
$I$	Identic matrix
$tr$	transpose operator
$u', v', w'$	turbulent component or vector velocity (m s <sup>-1</sup> )
$g$	magnitude of the acceleration (m s <sup>-2</sup> )
$T$	Temperature (K)
$T_u$	Turbulent intensity
$v_a$	Air velocity (m s <sup>-1</sup> )
$\Delta T$	Temperature difference (°C)
$T_f$	Floor temperature (°C)
$T_{mean}$	Mean static air temperature (°C)
$T_{MR}$	Mean radiant temperature (°C)
$T_{op}$	Mean operative temperature (°C)

### References

- Lee, E. Indoor environmental quality (IEQ) of LEED-certified home: Importance-performance analysis (IPA). *Build. Environ.* **2019**, *149*, 571–581. [[CrossRef](#)]
- Al horr, Y.; Arif, M.; Kafatygiotou, M.; Mazroei, A.; Kaushik, A.; Elsarrag, E. Impact of indoor environmental quality on occupant well-being and comfort: A review of the literature. *Int. J. Sustain. Built Environ.* **2016**, *5*, 1–11. [[CrossRef](#)]
- Rasheed, E.O.; Byrd, H. Can self-evaluation measure the effect of IEQ on productivity? A review of literature. *Facilities* **2017**, *35*, 601–621. [[CrossRef](#)]
- Murillo Camacho, K.S.; Fouseki, K.; Altamirano Medina, H. Decision-Making Processes of Residents in Preservation, Thermal Comfort, and Energy Efficiency in Heritage Buildings: A Pilot Study in Mexico City. *Appl. Sci.* **2022**, *12*, 1486. [[CrossRef](#)]
- Chow, T.T.; Fong, K.F.; Givoni, B.; Lin, Z.; Chan, A.L.S. Thermal sensation of Hong Kong people with increased air speed, temperature and humidity in air-conditioned environment. *Build. Environ.* **2010**, *45*, 2177–2183. [[CrossRef](#)]
- Zhuang, R.; Li, X.; Tu, J. CFD study of the effects of furniture layout on indoor air quality under typical office ventilation schemes. *Build. Simul.* **2014**, *7*, 263–275. [[CrossRef](#)]
- Ealiwa, M.A.; Taki, A.H.; Howarth, A.T.; Seden, M.R. An investigation into thermal comfort in the summer season of Ghadames, Libya. *Build. Environ.* **2001**, *36*, 231–237. [[CrossRef](#)]
- Zagorskis, J.; Zavadskas, E.K.; Turskis, Z.; Burinskienė, M.; Blumberga, A.; Blumberga, D. Thermal insulation alternatives of historic brick buildings in Baltic Sea Region. *Energy Build.* **2014**, *78*, 35–42. [[CrossRef](#)]

9. Shahzad, S.; Calautit, J.K.; Aquino, A.I.; Diana S.N.M.; Nasir, D.S.N.M.; Hughes, B.R. A user-controlled thermal chair for an open plan workplace: CFD and field studies of thermal comfort performance. *Appl. Energy* **2017**, *207*, 283–293. [[CrossRef](#)]
10. Awwad, A.; Mohamed, M.H.; Fatouh, M. Optimal design of a louver face ceiling diffuser using CFD to improve occupant's thermal comfort. *J. Build. Eng.* **2017**, *11*, 134–157. [[CrossRef](#)]
11. Mashita, T.; Kanayama, T.; Ratsamee, P. Personal Atmosphere: Estimation of Air Conditioner Parameters for Personalizing Thermal Comfort. *Appl. Sci.* **2020**, *10*, 8067. [[CrossRef](#)]
12. Balocco, C. Daily natural heat convection in a historical hall. *J. Cult. Herit.* **2007**, *8*, 370–376. [[CrossRef](#)]
13. Balocco, C.; Grazzini, G. Plant refurbishment in historical buildings turned into museum. *Energy Build.* **2007**, *39*, 693–701. [[CrossRef](#)]
14. Corgnati, S.P.; Perino, M. CFD application to optimise the ventilation strategy of Senate Room at Palazzo Madama in Turin (Italy). *J. Cult. Herit.* **2013**, *14*, 62–69. [[CrossRef](#)]
15. Jahanbin, A.; Semprini, G. Numerical Study on Indoor Environmental Quality in a Room Equipped with a Combined HRV and Radiator System. *Sustainability* **2020**, *12*, 10576. [[CrossRef](#)]
16. Jahanbin, A. Efficacy of coupling heat recovery ventilation and fan coil systems in improving the indoor air quality and thermal comfort condition. *Energy Built Environ.* **2022**, *3*, 478–495. [[CrossRef](#)]
17. Siemens Industries Digital Software. Simcenter STAR-CCM+ Academic Power on Demand. Available online: <https://plm.sw.siemens.com/en-US/simcenter/fluids-thermal-simulation/star-ccm/> (accessed on 6 February 2023).
18. Semprini, G.; Jahanbin, A.; Pulvirenti, B.; Guidorzi, P. Evaluation of Thermal Comfort Inside an Office Equipped with a Fan Coil HVAC System: A CFD Approach. *Future Cities Environ.* **2017**, *5*, 14. [[CrossRef](#)]
19. Lardeau, S.; Manceau, R. Computations of Complex Flow Configurations Using a Modified Elliptic-Blending Reynolds-Stress Model. In Proceedings of the 10th International ERCOFTAC Symposium on Engineering Turbulence Modelling and Measurements, Marbella, Spain, 17–19 September 2014.
20. Siegel, R.; Howell, J.R. *Thermal Radiation Heat Transfer*; Taylor & Francis: Washington, DC, USA, 1992.
21. ISO 7730:2005; Ergonomics of the Thermal Environment. International Organization for Standardization: Geneva, Switzerland, 2005. Available online: <https://www.iso.org/standard/39155.html> (accessed on 9 September 2022).
22. Fanger, O. *Thermal Comfort*; PLEA: Copenhagen, Denmark, 1970.
23. Maiti, R. PMV model is insufficient to capture subjective thermal response from Indians. *Int. J. Ind. Ergon.* **2014**, *44*, 349–361. [[CrossRef](#)]
24. Rupp, R.F.; Ghisi, E. Predicting thermal comfort in office buildings in a Brazilian temperate and humid climate. *Energy Build.* **2017**, *144*, 152–166. [[CrossRef](#)]
25. Mui, K.W.; Wong, L.T. Neutral temperature in subtropical climates—A field survey in air-conditioned offices. *Build. Environ.* **2007**, *42*, 699–706. [[CrossRef](#)]
26. Ren, J.; Liu, J.; Zhou, S.; Kim, M.K.; Miao, J. Developing a collaborative control strategy of a combined radiant floor cooling and ventilation system: A PMV-based model. *J. Build. Eng.* **2022**, *54*, 104648. [[CrossRef](#)]
27. Rupp, R.F.; Kazanci, O.B.; Toftum, J. Investigating current trends in clothing insulation using a global thermal comfort database. *Energy Build.* **2021**, *252*, 111431. [[CrossRef](#)]
28. Tartarini, F.; Schiavon, S. pythermalcomfort: A Python package for thermal comfort research. *SoftwareX* **2020**, *12*, 100578. [[CrossRef](#)]
29. Guidorzi, P.; Pompoli, F.; Bonfiglio, P.; Garai, M. A newly developed low-cost 3D acoustic positioning system: Description and application in a reverberation room. *Appl. Acoust.* **2020**, *160*, 107127. [[CrossRef](#)]

**Disclaimer/Publisher's Note:** The statements, opinions and data contained in all publications are solely those of the individual author(s) and contributor(s) and not of MDPI and/or the editor(s). MDPI and/or the editor(s) disclaim responsibility for any injury to people or property resulting from any ideas, methods, instructions or products referred to in the content.